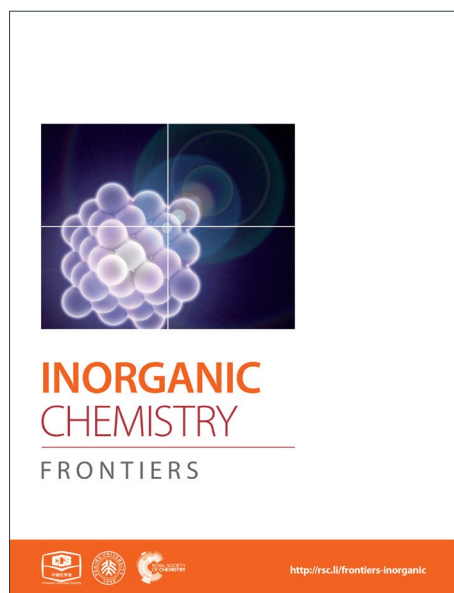
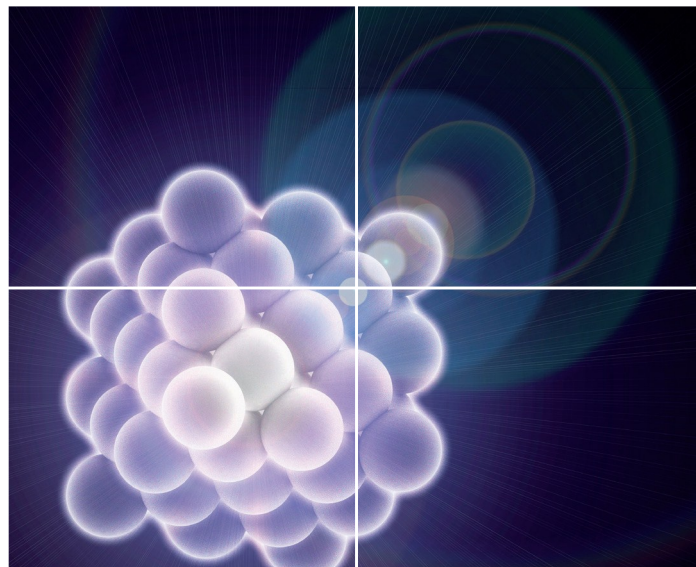


INORGANIC CHEMISTRY

FRONTIERS

Accepted Manuscript



This is an *Accepted Manuscript*, which has been through the Royal Society of Chemistry peer review process and has been accepted for publication.

Accepted Manuscripts are published online shortly after acceptance, before technical editing, formatting and proof reading. Using this free service, authors can make their results available to the community, in citable form, before we publish the edited article. We will replace this *Accepted Manuscript* with the edited and formatted *Advance Article* as soon as it is available.

You can find more information about *Accepted Manuscripts* in the [Information for Authors](#).

Please note that technical editing may introduce minor changes to the text and/or graphics, which may alter content. The journal's standard [Terms & Conditions](#) and the [Ethical guidelines](#) still apply. In no event shall the Royal Society of Chemistry be held responsible for any errors or omissions in this *Accepted Manuscript* or any consequences arising from the use of any information it contains.



Journal Name

ARTICLE

An Asymmetric Binuclear Zinc(II) Complex with Mixed Iminodiacetate and Phenanthroline Ligands: Synthesis, Characterization, Structural Conversion and Anticancer Properties

Received 00th January 20xx,
Accepted 00th January 20xx

DOI: 10.1039/x0xx00000x

www.rsc.org/

Lubin Ni,^{†a} Juan Wang,^{‡b} Chang Liu,^b Jinhong Fan,^b Yun Sun,^{*b} Zhaohui Zhou,^{*c} Guowang Diao,^{*a}

Transition metal complexes with substituted high affinity mixed ligands as potential anticancer agents can overcome the drawbacks of platinum-based drugs that are currently marketed. Here, a new water-soluble asymmetric binuclear iminodiacetato-zinc(II) complex $[\text{Zn}_2(\text{ida})(\text{phen})_3(\text{NO}_3)] \cdot \text{NO}_3 \cdot 5\text{H}_2\text{O}$ (**1**) with phenanthroline ligand has been synthesized and fully characterized with a wide range of analytical techniques including single crystal X-ray diffraction as well as spectroscopic techniques, such as FT-IR, UV/Vis, photoluminescence spectroscopy, and furthermore by elemental and thermogravimetric analysis. Moreover, unprecedented $(\text{H}_2\text{O})_{10}$ water clusters consisting of quasi-planar tetramer and six dangling water molecules were observed in the voids space of 3D supramolecular assemblies. The conversion behavior of (**1**) into two monomeric species $[\text{Zn}(\text{ida})(\text{phen})(\text{H}_2\text{O})]$ (**2**) and $[\text{Zn}(\text{phen})_2(\text{H}_2\text{O})_2]^{2+}$ (**3**) in aqueous solution was first studied by solid-state/solution NMR, ESI-MS, and solution UV/vis spectra. Next, these zinc (II) complexes (**1-3**), mixture of (**2**) and (**3**) (mole ratio 1/1), and ligands (phen and ida) were further evaluated for *in vitro* cytotoxic profile in human hepatoma cell lines (HepG2 and SMMC-7721). We found that complex (**1**) effectively inhibited the proliferation of hepatocellular carcinoma cells, which is similar with mixture of (**2**) and (**3**) in a 1:1 molar ratio, and IC_{50} values of (**1**) were almost about 20-50% of (**2**) or (**3**). Therefore, this binuclear complex (**1**) mainly acts a cooperative inhibitor with complexes (**2**) and (**3**) toward tumor growth in solution. We further extended preliminary research of complex (**1**) and found (**1**) could induce cell cycle arrest at the G0/G1 phase. Additionally, overdosing on (**1**) exhibited low toxicity of mice (LD_{50} of (**1**) in ICR mice = 736 mg/kg, with 95% confidence interval 635-842 mg/kg). In conclusion, complex (**1**) with high antitumor activity and low toxicity provides a new strategy for the treatment of liver cancer.

Introduction

Cancer, as a leading cause of death worldwide, has become a major health problem of global concern.^[1] As is well known, transition metal based drugs play a central role in antitumor chemotherapy, although the underlying relationship between molecular structures and their biological activities has not yet been completely interpreted so far.^[2] Platinum-based drugs such as cisplatin, carboplatin, and oxaliplatin, etc. have achieved the great successes in the treatment of various cancers.^[3-4] However, they induce

strong side effects including nephrotoxicity, emetogenesis and neurotoxicity during therapy.^[5] Therefore, design and synthesis of novel non-platinum metal complexes with high antitumor activity and less toxicity are in the focus of global interests.^[6-7]

Zinc (II) is an important essential trace element for organisms, and main building part of a series of enzymatic systems due to the physiological roles. Therefore, one present strategy was successfully illustrated by new Zn(II) coordination complexes with low toxicity in medicinal therapeutic applications,^[8] for treating diabetes mellitus^[9] or cancer.^[10-11] Another strategy in such ongoing efforts is to synergies the beneficial effect of high affinity and biologically relevant ligands for enhancing anticancer activity of transition metal complexes. Recently, potential biologically active moieties, such as 1,10-phenanthroline (phen) and aminocarboxylic acids, have been extensively involved in new-type drug design because of their unique properties.^[12] Phen is a classic nitrogen-chelating bidentate ligand, which displays strong cooperativity in cation binding to form stable transition metal complexes in solution. Phen and its derivatives are capable of high specific DNA intercalation-binding affinities owing to its rigid electron-deficient heteroaromatic rings.^[13] Aminocarboxylic acids having good biocompatibility as secondary ligand can further enhance the affinity of mixed-ligand

^a College of Chemistry and Chemical Engineering, Yangzhou University, Yangzhou 225002, Jiangsu, People's Republic of China. Email: gwdiao@yzu.edu.cn

^b College of Medicine, Yangzhou University, Yangzhou 225001, People's Republic of China. Email: ysun@yzu.edu.cn

^c State Key Laboratory for Physical Chemistry of Solid Surfaces, College of Chemistry and Chemical Engineering, Xiamen University, Xiamen 361005, People's Republic of China. Email: zhzhou@xmu.edu.cn

[†]Electronic Supplementary Information (ESI) available: crystallographic data, selected bond lengths and angles, hydrogen bonds, X-ray powder diffraction pattern, FT-IR and ¹H NMR spectra, thermogravimetric analysis (TGA) for compound (**1**), Hematological parameters in mice treated with (**1**) after 2 weeks. CCDC 1401929. For ESI and crystallographic data in CIF or other electronic format See DOI: 10.1039/x0xx00000x.

[‡] These authors contributed equally.

complexes towards DNA through the formation of hydrogen bonding between the ligands and the DNA molecules.^[14]

We are therefore interested in investigating an association of Zn(II)-containing structural motifs with some potent biologically active ligands would result in novel efficient chemotherapeutic agents against human cancers. There have been some reported studies on the crystal structure and their biochemical properties of phenanthroline zinc (II) complexes with aminocarboxylic acids.^[12, 15] However, phenanthroline dinuclear zinc (II) complexes substituted by iminodiacetate ligand has never been documented to date. Moreover, no studies on the conversion behavior of phenanthroline dinuclear zinc (II) complexes with aminocarboxylic acids in solution have been reported. Herein we report synthetic routes, characterization, structural conversion and anticancer properties of a novel water-soluble dimeric phenanthroline iminodiacetate zinc (II) complex $[\text{Zn}_2(\text{ida})(\text{phen})_3(\text{NO}_3)]\cdot\text{NO}_3\cdot 5\text{H}_2\text{O}$ (**1**) that stabilized the unprecedented decameric water cluster. The conversion behavior of this dimer (**1**) into two monomeric species $[\text{Zn}(\text{ida})(\text{phen})(\text{H}_2\text{O})]$ (**2**) and $[\text{Zn}(\text{phen})_2(\text{H}_2\text{O})_2]^{2+}$ (**3**) in aqueous solution was also first thoroughly investigated. Furthermore, complex (**1**) significantly inhibits the proliferation of human hepatoma cell lines and overdosing on complex (**1**) of mice exhibits low toxicity *in vivo*. The monomeric dissolved species (**2**) and (**3**) exerts a synergistic inhibitory effect on tumour cell growth in solution of complex (**1**).

Experimental

Reagents.

All Chemicals and reagents in this study were reagent grades and used without further purification. Dulbecco's modified Eagle's medium (DMEM) was purchased from Thermo Scientific (HyClone, Logan, UT, USA). Fetal bovine serum (FBS) was purchased from Wisent (Quebec, Canada). 3-(4,5-dimethylthiazol-2-yl)-2,5-diphenyltetrazolium bromide (MTT) was purchased from Sigma Chemical Co. (St. Louis, MO, USA). Phosphate-Buffered Saline (PBS) and Penicillin-Streptomycin Solution were from Beyotime Institute of Biotechnology (Shanghai, China).

Materials and physical measurements.

Elemental analyses (C, H and N) were performed using EA 1110 elemental analyzer. Fourier transform infrared (FT-IR) spectra were recorded on a Bruker Optics Vertex 70 Spectrometer. Solution ¹³C {1H} NMR spectra were measured on a Bruker Avance AV-400M Hz resonance spectrometer with D₂O solvent using DSS (sodium 2,2-dimethyl-2-silapentane-5-sulfonate) as an internal reference at room temperature. Solid ¹³C NMR spectra were recorded on a Bruker AV 400 NMR spectrometer using cross polarization, magic angle spinning (12 kHz) and Hexamethylbenzene (HMB) as the reference. Thermogravimetric analyses (TG) were collected with a Netzsch TG209 F1 instrument with a 10 °C min⁻¹ from 30 to 800 °C in flowing air atmosphere. UV/vis spectra were recorded on a Perkin-Elmer Lambda 650S spectrometer. Photoluminescence measurements were performed on a Perkin-Elmer LS 50B spectrometer. The X-ray powder diffraction patterns (XRD) were recorded on a Philips X'Pert PRO diffractometer, operated at 40 kV and 30mA using a Cu-target tube. High mass accuracy ESI spectra

were recorded on an ultrahigh-resolution ESI-Time-Of-Flight (Bruker Daltonik maxis (Bremen, Germany)). Spectra were obtained in positive-ion mode, with the capillary held at 4000 V. Complex (**1**) was dissolved in a H₂O/MeCN mixture (80:20) to enhance peak intensity.

Synthesis of $[\text{Zn}_2(\text{ida})(\text{phen})_3(\text{NO}_3)]\cdot\text{NO}_3\cdot 5\text{H}_2\text{O}$ (**1**).

0.67 g (5mmol) of iminodiacetic acid was dissolved in 25 ml of deionized water with stirring. 1.49 g (5mmol) of Zinc nitrate hexahydrate and 1.01 g (5 mmol) 1,10-phenanthroline were slowly added to the reaction mixture, and the mixture was left stirring for 30 min. Next, the solution pH value was adjusted to 2.0~3.0 by 1.0 M ammonia and then filtered. Slow evaporation of the solution afforded colorless single crystals of (**1**) after approx one week. Yield 2.88g (57% based on Zn). Ft-IR (KBr, cm⁻¹): $\nu_{\text{as}}(\text{COO})$ 1618(vs), 1584(vs); $\nu_{\text{s}}(\text{COO})$ 1518(m), 1426(m), 1382(s), 1320(m). Solution ¹H NMR (400 MHz, D₂O): 3.98 (1H, d, *J* = 10.0 Hz), 3.40 (1H, d, *J* = 9.6 Hz), 9.27 (s, 1H), 8.94(2H, t, *J* = 5.2 Hz), 8.87 (s, 1H), 8.75(m, 1H) 8.52 (s, 1H), 8.38 (s, 1H), 8.29(s, 1H), 8.14(2H, d, *J* = 14.0 Hz), 8.02(2H, d, *J* = 20.0 Hz). Solution ¹³C NMR (400 MHz, D₂O): δ_{c} (ppm) 182.3(CO₂), 56.4(CH₂). Solid-state ¹³C NMR: δ_{c} (ppm) 183.4(CO₂), 177.2(CO₂), 55.7(CH₂), 53.8(CH₂). Elemental analysis calcd. (found): C 47.26 (47.13); H 3.87 (3.82); N, 12.40 (12.28).

Synthesis of $[\text{Zn}(\text{ida})(\text{phen})(\text{H}_2\text{O})]\cdot 2\text{H}_2\text{O}$ (**2**).

Complex (**2**) was freshly prepared according to the literature.^[15] Reaction of zinc chloride (0.68g, 5.0mmol), iminodiacetic acid (0.67g, 5.0 mmol) and 1,10-phenanthroline (1.01g, 5.0 mmol) at pH 7.0 results in a yield of 0.99g(46%).

Synthesis of $[\text{Zn}(\text{phen})_2(\text{H}_2\text{O})_2]\text{SO}_4\cdot 6\text{H}_2\text{O}$ (**3**).

The complex was obtained from an aqueous acetone solution of ZnSO₄·7H₂O (1mmol, 0.287mg) and 1,10-phenanthroline (2mmol, 0.396mg) in a molar ratio of 1:2. Slow evaporation of the solution afforded colorless single crystals of (**3**) (Yield 209 mg, 32%) after approx two days. The crystal structure of complex (**3**) has been first reported by Liu *et al.* in 2001.^[16]

X-ray crystallography.

Data collections of (**1**) was performed on an Oxford Gemini Sultra system with graphite mono-chromate (MoK α radiation, λ = 0.71073 Å) at 173K. Routine Lorentz and polarization corrections were applied, and an absorption correction was performed using the program *CrysAlis* (multi-scan).^[17] The structure was solved using the WinGXpackage^[18] and refined by full-matrix least-squares procedures with anisotropic thermal parameters for all the non-hydrogen atoms using SHELXL-97.^[19] Hydrogen atoms were included and located from difference Fourier maps but not refined anisotropically.

Cell culture.

Human hepatoma cell lines HepG2 and SMMC-7721 were purchased from the Cell Bank of the Chinese Academic of Sciences (Shanghai, P. R. China). The cells were maintained at 37 °C at 5% CO₂ in DMEM medium containing 10% FBS, and Penicillin-Streptomycin Solution.

Cell viability.

Cell viabilities were determined by MTT assay as described previously.^[20] Cells were plated at density of 1×10^4 per well. After cultured overnight, cells were treated with either vehicle control or various concentrations of (1-3), mixture of (2) and (3) (molar ratio 1/1), ligands (phen and ida), ZnCl_2 and ZnSO_4 . After incubation for 24 or 48 h, cells each well were added to $10 \mu\text{l}$ of MTT solution (5 mg/ml) and incubated for an additional 4h. After incubation, media was instead of $100 \mu\text{l}$ DMSO to dissolve purple precipitates. Absorbance was detected at 570 nm by a microplate spectrophotometer (Bio-tek, Inc). The effects of (1-3), mixture of (2) and (3), ligands (phen and ida), ZnCl_2 and ZnSO_4 on cells proliferation were assessed as the percentage of cell growth (vehicle-treated cells were taken as 100% viable).

Cell cycle analysis.

Cells were plated at density of 2×10^6 in 150mm culture dishes, and treated with vehicle control or various concentrations of (1) for 48h. Cells were harvested and fixed in 70% ice-cold methanol for 12h at 4°C . After trypsinized, cells were washed with PBS and fixed in 95% ethanol at 4°C overnight followed by 10 mg/ml RNase and 1 mg/ml Propidium Iodide (Boyttime, Jiangsu, P. R. China). Flow cytometric analysis was performed using a flow cytometry system (BD FACSCalibur, USA). The data were analyzed using the ModifitLT V2.0. software (Verity Software House, Topsham, ME).

Ethics statement.

All animal experiments in this study were approved by the Institutional Animal Care and Use Committee of Yangzhou University and handled following the International Animal Ethics Committee Guidelines, ensuring minimum animal suffering.

Animal.

Thirty male ICR mice and 30 female mice, aged 5 weeks, weighting $18 \pm 2\text{g}$, were purchased from Yangzhou University Comparative Medicine Center (License No: SCXK (Su) 20120009) and acclimatized under standard conditions for laboratory animals: a temperature of $23 \pm 2^\circ\text{C}$, a relative humidity of $50 \pm 5\%$, and a 12-hour light/dark cycle.

Single-dose acute toxicity testing.

All mice were fasted for 6 h prior to conducting the experiment. This study was conducted over 15 days (days 0–14). Briefly, all mice were randomly divided into six groups of ten each (five males and five females). On day 0, the mice were intragastrically administered (1). The doses were 1500, 1125, 844, 632, or 474 mg/kg. In the control group, ten mice (five males and five females) were intragastrically administered with double distilled water. The mice were observed individually for signs of acute toxicity and behavioral changes for 4 h post dosing and at least once daily for 14d. The mortality rate of the mice was recorded to calculate the LD_{50} values. Histopathological and hematological of examination, and ALT and BUN levels of determination on mice were performed for all mice alive on day 14. The main processes in this study are as follows (Scheme 1):



Scheme. 1 illustrations of single-dose acute toxicity testing.

Statistical analysis.

All values are expressed as means \pm the standard error of the mean (S.E.M). Statistical analysis was performed using one-way analysis of variance for multiple comparisons, followed by Student-Newman-Keuls test to evaluate the significance of differences between two groups. A p -value less than 0.05 is considered statistically significant.

Results and Discussion

Synthesis and Crystal Structure.

Complex (1) was successfully synthesized by reacting zinc nitrate together with iminodiacetic acid (H_2ida) and 1,10-phenanthroline (phen) ligands at the low pH (2.0~3.0) in a molar ratio of 1:1:1 (Fig. 1a). In our preceding studies, the monomeric phenanthroline iminodiacetato zinc(II) complex $[\text{Zn}(\text{ida})(\text{phen})(\text{H}_2\text{O})] \cdot 2\text{H}_2\text{O}$ (2) was obtained at the higher pH of 7.0 (Fig. 1b).^[15] Therefore, these results exhibit the pH-dependent assembly of two phenanthroline iminodiacetato zinc (II) complexes.

The composition of (1) was determined from X-ray crystallography data in combination with elemental and thermogravimetric analyses (Table S1). The phase purity of (1) obtained was also confirmed with Powder X-ray diffraction (PXRD) measurements (Fig. S2). Complex (1) was further thoroughly characterized by infrared (FT-IR) and UV/vis spectra, electrospray ionization mass spectrometry (ESI-MS), ^1H and ^{13}C NMR spectroscopy, and photoluminescence spectroscopy (PL). Selected bond lengths and angles are listed in Table S2.

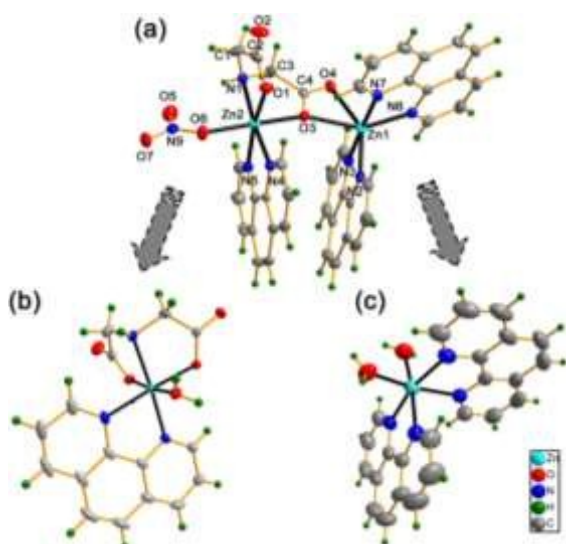


Fig. 1 X-ray crystallographic structures of (a) zinc(II) dimeric complex $[\text{Zn}_2(\text{ida})(\text{phen})_3(\text{NO}_3)]^+$ cation (**1**), (b) zinc(II) monomeric complex $[\text{Zn}(\text{ida})(\text{phen})(\text{H}_2\text{O})] \cdot 2\text{H}_2\text{O}$ (**2**) and (c) phenanthroline zinc(II) complex $[\text{Zn}(\text{phen})_2(\text{H}_2\text{O})_2]\text{SO}_4 \cdot 6\text{H}_2\text{O}$ (**3**) with ellipsoids set at 50% probability. One counter nitrate anion in (**1**), one counter sulfate anion in (**3**) and solvent water molecules in (**1**)-(3) have been omitted for clarity.

The crystallographic asymmetric unit of (**1**) contains one $[\text{Zn}_2(\text{ida})(\text{phen})_3(\text{NO}_3)]^+$ monocation, one nitrate ion as counterion and five solvent water molecules. The molecular structure of $[\text{Zn}_2(\text{ida})(\text{phen})_3(\text{NO}_3)]^+$ cation (**1**) along with the atomic numbering scheme is shown in Fig. 1a. Each Zn(II) ion has a distorted octahedral geometry. The Zn(1) atom is six-coordinated by four nitrogen atoms from two phen ligands and two oxygen atoms from the same carboxy group of ida ligand, with N(3), N(6), N(7) and O(3) atoms in equatorial plane and N(2), O(4) atoms at the apical positions. The Zn(2) atom is surrounded by the third phen ligand, one unidentate nitrate and an O,N,O'-tridentate chelating ida ligand. The N(4), N(5) atoms from phen ligand, the imine N(1) atom and one carboxy O(1) atom of the ida ligand constitute the equatorial plane, while the O(6) atom of a nitrate and the bridging atom O(3) from carboxy group of ida ligand occupy the axis points. It is noticeable that the distances of Zn(1)-O(3) and Zn(1)-O(4) [2.314(1) and 2.210(1) Å] are much longer in the iminodiacetato zinc complexes reported [2.010(2)-2.209(3), Table S2 and S3].^[15,21] The two different coordinated moieties $[\text{Zn}(\text{phen})_2]^{2+}$ and $[\text{Zn}(\text{phen})(\text{NO}_3)]^+$ are thus connected *via* a bridging ida dianion, meanwhile the O(3) atom as another bridge directly linking to two Zn(II) ion [Zn(1)⋯Zn(2) 4.394(1) Å], forming an asymmetric binuclear zinc complex. Thus, the ida ligand plays a dual role of double-bridging and tetradentate agent in complex (**1**).

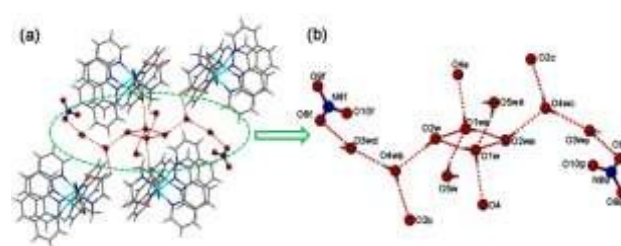


Fig. 2 (a) Perspective view of the discrete decameric water cluster $(\text{H}_2\text{O})_{10}$; (b) The $(\text{H}_2\text{O})_{10}$ cluster gathering four neighbouring units of complex (**1**) by hydrogen-bonding interactions viewed down *x* axis. Symmetry codes: a, $1-x, 1-y, 1-z$; b, $-x, 1-y, 1-z$; c, $1+x, y, z$; d, $x, 3/2-y, 1/2+z$; e, $1-x, y-1/2, 1/2-z$; f, $x, 1/2-y, 1/2+z$; g, $1-x, 1/2+y, 1/2-z$. Color code: red atom (oxygen); blue atom (nitrogen); gray atom (hydrogen); red dash (H-bonding interactions).

Interestingly, the hydrogen-bonding interactions of five lattice water molecules of crystallization lead to formation of a new finite decameric water cluster $(\text{H}_2\text{O})_{10}$ intercalated in the void spaces of (**1**) (Fig. 2). Unprecedented $(\text{H}_2\text{O})_{10}$ cluster consists of a cyclic quasi-planar tetramer (O1w and O2w), and six dangling water molecules (O3w, O4w, O5w) (Fig. 2b). In $(\text{H}_2\text{O})_{10}$ cluster, O(1w) and O(4w) both act as a hydrogen-bond donor to nearby carboxy O atoms assembling four neighbouring $[\text{Zn}_2(\text{ida})(\text{phen})_3(\text{NO}_3)]^+$ units around each decameric water cluster (Fig. 2a). The adjacent O(w)⋯O(w) distances (2.679~2.934 Å, 2.82 Å on average, Table S4) are located in the reported range.^[22-23] The overall structure is further stabilized by intermolecular π - π interactions between the aromatic rings of phenanthroline entities with an average ring centroid-centroid separation of 3.63 Å. Moreover, C-H⋯O interactions play an important role in stabilizing particular structures of biomolecules such as nucleic acids, proteins, and carbohydrates in biochemistry.^[24] Complex (**1**) also displays strong C-H⋯O intermolecular interactions between phen H and carboxy O [C(21)⋯O(4) 3.232(2) Å, $\angle\text{C-H}\cdots\text{O}$ 153.9°, Table S4], which is further assembled into a 3D supramolecular framework (Fig. S1).

General Characterization.

Thermal gravimetric analysis of compound (**1**) showed a 7.20 % weight loss between 30 and 250 °C, corresponding to five lattice water molecules (calcd value: 8.85 %). From 250 °C to 800 °C, the anhydrous compound decomposed with stepwise loss of the organic ida and phen ligands, leading to the decomposition of the 3D frameworks into residual product zinc oxide (observed 15.9 %, calcd 14.5 %, JCPDS No. 36-1451) (Fig. S3). This was also further verified by PXRD patterns of bulk (**1**) calcined at different temperatures (Fig. S2). The FT-IR spectrum of (**1**) exhibited a broad absorption centered at 3425 cm^{-1} attributed to the O-H stretching frequency derived from the water cluster (Fig. S4). The sharp vibrations at 854 and 740 cm^{-1} are due to the $\delta_{(\text{C-H})}$ vibrations of the phen ligand.^[25] Typical carboxy stretching vibrations in (**1**) appear at 1614, 1587 and 1512 cm^{-1} for $\nu_{\text{as}}(\text{CO}_2)$ and at 1426, 1378, 1320 cm^{-1} for $\nu_{\text{s}}(\text{CO}_2)$.^[26] The separations between these signals ($\Delta\nu$) are 188, 209 and 192 cm^{-1} , respectively, suggesting that ida acts as both bidentate and unidentate ligands between two zinc atoms, which is consistent with crystallographic structure.

Solid-state/Solution UV-Vis spectroscopy and Fluorescent properties.

UV-vis diffuse reflectance spectra of complex **(1)** displays a set of intense absorption bands of 1,10-phen ligand in the UV region (208–326 nm), due to the absorption of ligand-centered $\pi-\pi^*$ transitions (Figure 3a).^[27] However, the electronic spectra of the complex **(1)** in water gives slightly different absorption peaks centered at 226 nm, 268 nm with one shoulder at 290 nm (Fig. 3b). The spectrum of the zinc complex **(1)** is almost overlapping with that of the free phen ligand, revealing allowed $\pi-\pi^*$ transitions. Nevertheless, the complexation of Zn^{2+} to phen ligand in **(1)** posed a small red shift in the absorbance maximum and a large increase in molar absorption coefficient (Fig. 3b, Table S5) compared to free phen ligand, probably due to the steric hindrance within the coordination cage of phen rings around the zinc cations.^[27]

Because Zn^{2+} is spectroscopically silent due to its d^{10} electron configuration, the design of fluorescent chemosensors for the detection of Zn^{2+} has been studied intensively.^[28] To further investigate the potential fluorescent properties of complex **(1)**, the photoluminescence spectra of **(1)** and free phen ligand were recorded in the solid-state and in aqueous solution at ambient temperature. Complex **(1)** exhibits intense photoluminescence in comparison with the free phen ligand (Figs. 3c-3d). The emission spectra displays two characteristic emission bands of two coordinated phen ligands at 375 and 393 nm ($\lambda_{\text{ex}} = 331$ nm in the solid state), at 367 and 383 nm ($\lambda_{\text{ex}} = 312$ nm in water). The two emission bands in **1** are neither metal-to-ligand charge transfer (MLCT) nor ligand-to-metal charge transfer (LMCT) in nature, since the closed d^{10} electronic shell configuration of Zn^{2+} cations leads to the absence of $d-d$ transitions in the photoemission spectra. Therefore, it can be assigned to the $\pi-\pi^*$ intraligand fluorescence of the 1,10-phenanthroline ligand.^[29] Compared with the emission peaks of two free ligands, a red-shifted emissions for **(1)** could be attributed to the cooperative effect of diverse weak interactions controlled by $\pi-\pi$ stacking and hydrogen bonds, leading to decrease the HOMO-LUMO energy gaps.^[30] The coordination of phen ligands to the zinc(II) ions effectively reduce the loss of energy *via* radiationless thermal vibrations by increasing the rigidity of the chromophore, thus enhancing photoluminescence emissions.^[30]

temperature ($C = 0.008$ mM); (c) Solid-state photoluminescence spectra of complex **(1)** and 1,10-phen at room temperature. The corresponding excitation wavelengths, λ_{ex} are 331, 340 nm, respectively; (d) Photoluminescence spectra of complex **(1)** and 1,10-phen in aqueous solution at room temperature. λ_{ex} are 312, 297 nm, respectively ($C = 0.1$ mM).

Transformation in aqueous solution.

The structural information and the conversions of **(1)** in aqueous media were investigated by solid/solution NMR spectroscopy, electrospray ionization-mass spectrometry (ESI-MS), and time-resolved UV-vis absorption spectra. Solid ^{13}C NMR spectrum of **(1)** is shown in Fig. 4a. The presence of two peaks at 183.4 and 177.2 ppm with downfield shift $\Delta\delta$ of 6.2 ppm can be ascribed to the monodentate and μ_2 -bridging carboxy carbons [C(2) and C(4), see Fig. 1a] of coordinated ida ligand, respectively. Moreover, two peaks at 55.7 and 53.8 ppm correspond to two methylene groups of ida.^[15] The other resonances in the range 128-151 ppm are attributed to the carbons of three coordinated phen rings. These results are in good agreement with the solid-state structure from X-ray crystallography data. However, the solution ^{13}C NMR spectrum of **(1)** is quite different from that in solid complex **(1)**. Only one set of ^{13}C resonances observed at 182.3 and 56.4 ppm are corresponding to the carboxy and methylene carbons of ida, respectively (Fig. 4b). In comparison with free ida ligand in solution at pH 2.0, both the ^{13}C NMR signals of carboxy and methylene carbons in **(1)** have large downfield shifts ($\Delta\delta$) 8.9 and 4.9 ppm, respectively (Fig. S6). The solution ^1H NMR spectrum of **(1)** contained two CH_2 signals from ida ligand observed at 3.98 and 3.40 ppm.^[15] The signals in the range 7.98-9.21 ppm are assigned to phen hydrogen atoms (Fig. S5).^[31] Based on the molecular structure of **(1)** in the solid state combined with solid ^{13}C NMR signals, there exist two types of coordination modes of carboxy groups, but only one peak was found for the carboxy groups in solution. This may result from the transformation of the dimeric complex **(1)** to the monomeric units in solution. To gain further insight into the conversion pathway of **(1)** in solution, we also investigated the ESI-MS spectrum of **(1)** in water (Fig. 4c). The spectrum showed base peak at m/z 537.05 that is equivalent to the monomeric phenanthroline iminodiacetato zinc (II) complex $[\text{Zn}(\text{ida})(\text{phen})(\text{H}_2\text{O})(\mathbf{2}) + 8\text{H}_2\text{O}]^+$, which might involve the removal of one electron from phenanthroline ligand to form a positive molecular ion M^+ . The other monovalent cationic peak centered at m/z 486.05 corresponds to monomeric phenanthroline zinc (II) species $[\text{Zn}(\text{phen})_2(\mathbf{3}) + (\text{NO}_3^-)]^+$. Therefore, solution ^{13}C NMR and ESI-MS results are consistent with a conversion pathway reaction of the dimeric complex **(1)** in aqueous solution. All these results indicate **(1)** undergoes transformation in solution at relatively weak bonded μ_2 -bridging carboxyl group, which can be easily attacked and substituted by water molecules arising from the bond cleavage of $\text{Zn}(1)-\text{O}(3)$ and $\text{Zn}(1)-\text{O}(4)$ associated with the leaving process of unidentate nitrate ion, leading to form two monomeric species $[\text{Zn}(\text{ida})(\text{phen})(\text{H}_2\text{O})](\mathbf{2})$ and $[\text{Zn}(\text{phen})_2(\text{H}_2\text{O})_2]^{2+}(\mathbf{3})$ (Fig. 4d).

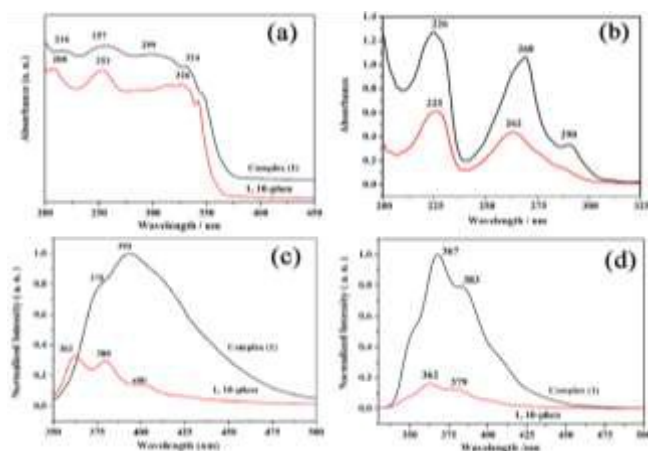


Fig. 3 (a) The diffuse reflectance absorption of complex **(1)** and 1,10-phenanthroline at room temperature; (b) UV-vis spectra of complex **(1)** and 1,10-phenanthroline in aqueous solution at room

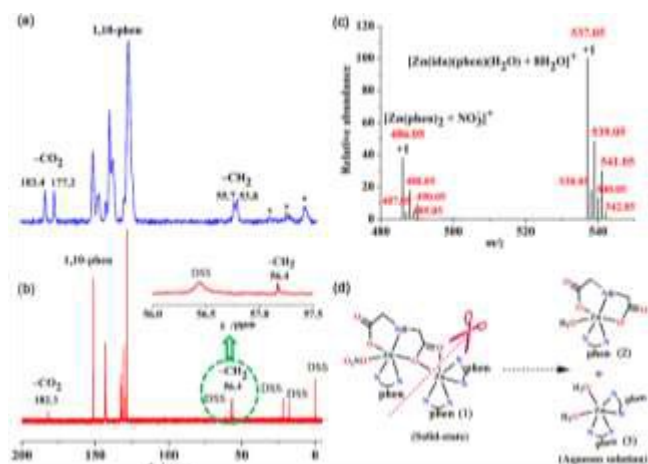


Fig. 4 (a) Solid ^{13}C NMR spectra of **(1)**, (* for spinning sidebands); (b) Solution ^{13}C NMR spectra of **(1)**, (inset: magnification of the methylene carbons ($-\text{CH}_2$) region); (c) ESI-MS spectra of **(1)** in positive ion mode; (d) Conversion of **(1)** into two different monomers in water.

Moreover, the time-resolved UV-vis absorption spectra of complex **(1)** in Phosphate-buffered Saline (PBS) buffer solution (pH=7.2) were recorded at 2 min intervals (Fig. S7a). The absorption spectra of two monomeric complexes $[\text{Zn}(\text{ida})(\text{phen})(\text{H}_2\text{O})]$ (**2**), $[\text{Zn}(\text{phen})_2(\text{H}_2\text{O})_2]\text{SO}_4$ (**3**), and their mixed species at 1:1 molar ratio in PBS buffer were also studied in Fig. S7b. The absorbance maximum of **(1)** is at the same wavelength as that of monomeric complex **(2)** or **(3)** but exhibits a significantly higher intensity (Fig. S7b). However, the mixed species of **(2)** and **(3)** at 1:1 molar ratio can show almost equivalent absorbance peak intensities, compared with complex **(1)** (Fig. S7b). In addition, almost no decrease in absorbance of complex **(1)** could be observed during 2 hour in PBS buffer (Fig. S7a), suggesting that the conversion of complex **(1)** into monomers **(2)** and **(3)** probably proceed very rapidly.

In Vitro Cytotoxicity

To evaluate the cytotoxic activity of complexes and ligands, human hepatoma cell lines (HepG2 and SMMC-7721) were incubated with various concentrations of the complexes **(1-3)**, mixture of **(2)** and **(3)** (1:1), ligands (phen and ida), ZnCl_2 and ZnSO_4 for 24 or 48h, respectively. We observed that all the complexes and ligands inhibited the proliferation of hepatoma cell lines in a dose-dependent manner (Figs. 5a-5d). A significant decrease of HepG2 cells viability has been detected at low concentrations, especially in the presence of complex **(1)** and mixture (**(2)** and **(3)**, 1:1 molar ratio). Interestingly, **(1)** and mixture showed a relevant cytotoxicity with IC_{50} of 10.01 ± 1.08 and 13.75 ± 3.39 μM after 48h, respectively, whereas **(2)** and **(3)** exhibited 50% of toxicity at higher concentrations (IC_{50} of 41.63 ± 1.75 and 22.34 ± 0.80 μM after 48h, respectively)(Fig. 5e). Similarly, the SMMC-7721 cells viability was significantly decreased in incubation with **(1)** and mixture at low concentrations (IC_{50} of 11.75 ± 1.75 and 12.58 ± 2.20 μM after 48 h, respectively). However, **(2)** and **(3)** were much less active against SMMC-7721 (IC_{50} = 44.36 ± 5.27 μM and 27.02 ± 2.78 μM after 48h, respectively). IC_{50} values of **(2)** or **(3)** were almost about 2~3 fold stronger than that of **(1)** or mixture of **(2)** and **(3)** at a 1:1 molar ratio. Complex **(1)** and mixture exerted similar 50% inhibited rate

from hepatoma cell lines further confirms complex **(1)** undergoes dissociation from dimer to two monomers **(2)** and **(3)** in solution. Hence, we inferred that binuclear **(1)** mainly acts an essential cooperative inhibitor with **(2)** and **(3)** toward tumor growth in solution.

Furthermore, ligands (phen and ida) had lower inhibited rates against hepatoma cell lines (Fig. 5e), compared to complexes **(1-3)**. Notably, zinc ion (ZnCl_2 and ZnSO_4) showed lower cytotoxic activity (IC_{50} values of ZnCl_2 and ZnSO_4 incubated with HepG2 and SMMC-7721 for 48h were all $>200\mu\text{M}$) (Fig. S8). Combined the above results, relative cytotoxic activities of complexes and ligands against human hepatoma cell lines are the following order: **(1)** \approx mixture (**(2)** and **(3)**, 1:1) $>$ **(3)**, **(2)** $>$ ida, phen $>$ ZnCl_2 , ZnSO_4 . All in all, effects of transition metal ion coordination, and the numbers and types of ligand can exert key influence on the evaluation of cytotoxicity. In short, complex **(1)** exerts similar antitumor activity (Table. S7) compared with the marked platinum-based drugs.^[32]

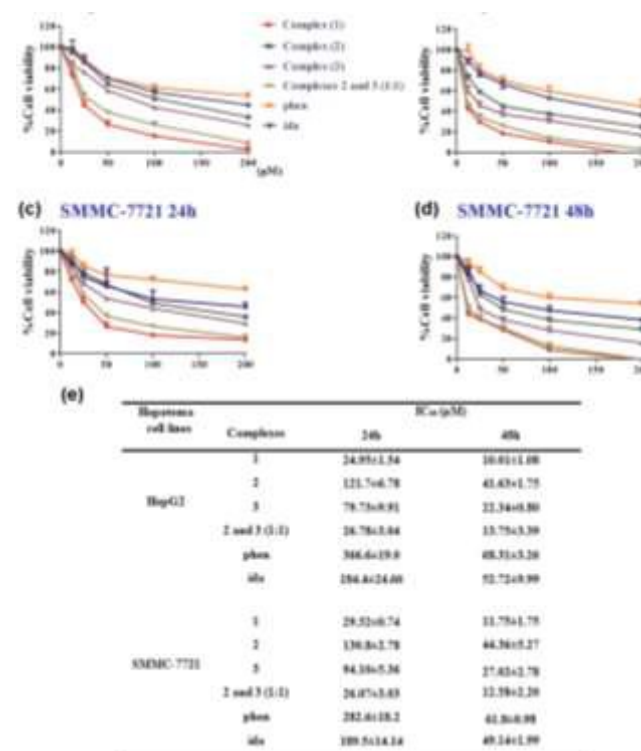


Fig. 5 Complexes and ligands inhibited the proliferation of hepatoma cell lines. (a-d) HepG2 and SMMC-7721 cells were incubated with various concentrations of complexes **(1-3)**, mixture of **2** and **3** (**1:1**), and ligands (phen and ida) for 24 or 48h, respectively. (e) IC_{50} values of complexes and ligands calculated on average values of % inhibition at various molecule concentrations. The results are presented as the means \pm S.E.M. of three independent experiments.

Cell Cycle Analysis

To further elucidate the possible mechanism that complex **(1)** inhibits cell growth, we tested the cell cycle arrest of hepatoma cell lines via flow cytometry after **(1)** treatment (Fig. 6a). Our results showed that untreated HepG2 and SMMC-7721 cells exhibited cell cycle profile after 48h in culture.^[33] As shown in Fig. 6b, complex **(1)**

could strongly induce HepG2 cells to undergo G0/G1 arrest after 48h, with a dose-dependent increase in the mean percentage ($78.02 \pm 3.25\%$ at $12.5\mu\text{M}$, $79.58 \pm 2.26\%$ at $25\mu\text{M}$, $80.35 \pm 4.65\%$ at $50\mu\text{M}$, $86.59 \pm 1.68\%$ at $100\mu\text{M}$) of cells compared with $57.70 \pm 3.36\%$ of cells in the control group in G0/G1. In addition, HepG2 cells population at S phase after (1) treatment significantly decreased ($16.13 \pm 1.09\%$ at $12.5\mu\text{M}$, $15.12 \pm 1.91\%$ at $25\mu\text{M}$, $14.27 \pm 1.19\%$ at $50\mu\text{M}$, $11.15 \pm 1.26\%$ at $100\mu\text{M}$) compared with $22.68 \pm 1.91\%$ of cells in the control group at S phase. Complex (1) also blocked cell into G2/M phase ($5.86 \pm 3.22\%$ at $12.5\mu\text{M}$, $5.31 \pm 3.07\%$ at $25\mu\text{M}$, $5.38 \pm 4.36\%$ at $50\mu\text{M}$, $2.26 \pm 1.55\%$ at $100\mu\text{M}$) compared with $19.63 \pm 2.97\%$ of cells in the control group at G2/M phase. Similarly, the SMMC-7721 cells population at G0/G1 after (1) treatment increased from $72.56 \pm 5.80\%$ (at $12.5\mu\text{M}$) to $84.50 \pm 4.18\%$ (at $100\mu\text{M}$) in a dose-dependent manner compared to that of control group which had a corresponding population of $58.78 \pm 4.50\%$ at G0/G1 (Fig. 6c). Moreover, S and G2/M phases of SMMC-7721 cells dropped significantly after treatment of complex (1), respectively. The data indicated complex (1) block cell progression into S and G2/M phases, and thus a certain proportion of cells is arrested at G0/G1.^[34-36]

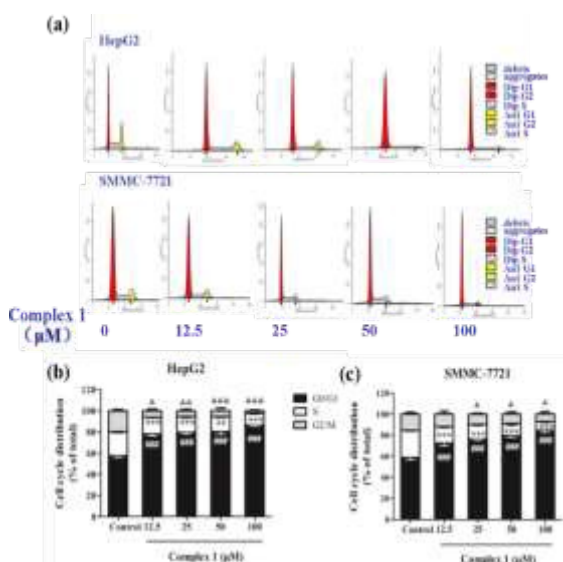


Fig. 6 Complex (1) affected cell cycle distribution of hepatoma cell lines. (a) HepG2 and SMMC-7721 cells were treated with 0, 12.5, 25, 50 and $100\mu\text{M}$ of complex (1) for 48h followed by staining with propidium iodide for flow cytometric analysis. (b-c) Graphs depict the cell distribution in the different phases of the cell cycle determined by flow cytometry, and bar charts present the percentage of cells in the indicated phase of cell cycle. The results are presented as the means \pm S.E.M. of three independent experiments. ### $p < 0.001$ compared with the control group at the G0/G1 phase; *** $p < 0.001$ compared with the control group at the S phase; & $p < 0.05$, && $p < 0.01$, &&& $p < 0.001$ compared with the control group at the G2/M phase.

Acute Toxicity

Safety is another primary concern when considering new drug candidates intended for use in human.^[37] Acute toxicity studies may also aid in the selection of starting doses for phase I clinical studies and provide information relevant to acute overdosing in human.^[6] We thus examined *in vivo* toxicity profile of complex (1). As shown in Fig. 7a, the median lethal dose (LD_{50}) value of (1) in ICR mice is

736 mg/kg by intragastrical administration, with the 95% confidence limits of $635\text{--}842 \text{ mg/kg}$. Notably, complex (1) is administrated by *i.g.* and has lower toxicity than the marked platinum-based drugs that exert antitumor activity only by *i.p.* (Table. S8).^[38]

Alanine transaminase (ALT) and blood urea nitrogen (BUN) are two important factors used to evaluate liver and kidney functions, respectively.^[39] Serum ALT level showed a slight, dose-dependent increase in the groups treated with (1) (Fig. 7b). However, treatment of (1) even at dose of 474 mg/kg or 632 mg/kg manifested no significant differences when compared with the control group. As shown in Fig. 7c, treatment of (1) significantly increased serum BUN level in male mice compared with the control male mice. Similarly, compared with control female mice, treatment of (1) at 632 mg/kg significantly increased serum BUN level in female mice, which implied that (1) at a dose of 632 mg/kg has possible kidney toxicity on mice.

Histopathology is an important factor for determining the treatment performance and effects, especially the negative effects.^[40] To further explore potential toxicity of (1), we conducted the histopathological evaluation with H&E staining. These results showed no significant evidence of tissues toxicity on mice alive treated with (1) at a dose of 632 mg/kg (Fig. 7d). Notably, there was no significant kidney change on mice treated with (1) at a dose of 632 mg/kg . These data documented treatment of (1) has no significant toxicity on the critical organs of mice.

In the hematology parameters, the oral administration of (1) did not remarkably affect the blood hematologic parameters of mice, because most parameters are within in physiological range (Table S6). However, a statistically decrease of hemoglobin was observed in the group treated with (1) at dose of 474 mg/kg and 632 mg/kg both in male and female mice ($p < 0.01$, $p < 0.01$, $p < 0.05$, $p < 0.01$, respectively). Additionally, the white blood cells in mice treated with (1) were significantly increased in comparison to that of the control group ($p < 0.01$, $p < 0.01$, $p < 0.01$, $p < 0.001$, respectively). Therefore, we inferred that overdosing on complex (1) might possess lower bone marrow toxicity in mice.

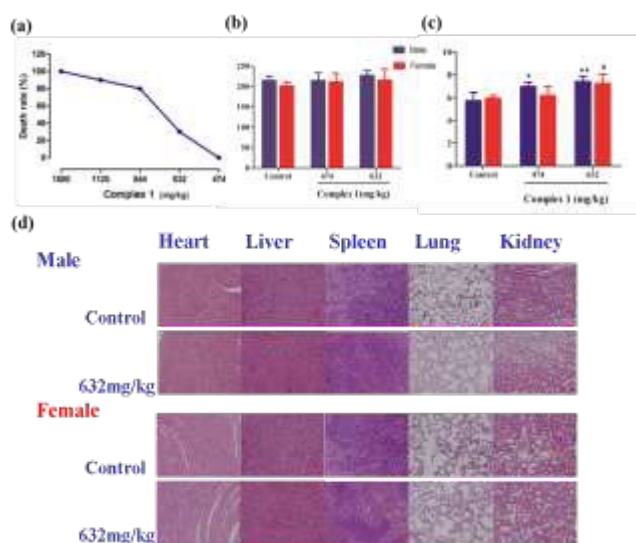


Fig. 7 (a) Dose-dependent manner of the complex (1) effects on the mice death. LD₅₀ of complex (1) = 736 mg/kg (95% confidence interval 635-842 mg/kg). Serum ALT (b) and BUN (c) levels in mice treated with complex (1) at various concentrations. (d) Histological examinations included heart, liver, spleen, lung and kidney sections in mice alive after administration with a single dose of (1) 632 mg/kg (200×). The results are presented as the means ± S.E.M. *p < 0.05, #p < 0.01 compared with the male control group; #p < 0.05 compared with the female control group.

Conclusions

In summary, we have synthesized and fully characterized a novel water-soluble asymmetric binuclear zinc (II) complex [Zn₂(ida)(phen)₃(NO₃)]·NO₃·5H₂O (1) with mixed ligands of iminodiacetate and 1, 10-phenanthroline. The interesting result is the discovery of a novel decameric water cluster (H₂O)₁₀, which was further connected neighboring [Zn₂(ida)(phen)₃(NO₃)]⁺ cation into a 3D supramolecular network via extensive hydrogen bonding. The structural conversion of (1) into two monomeric species [Zn(ida)(phen)(H₂O)] (2) and [Zn(phen)₂(H₂O)₂]⁺ (3) in water was illustrated. Next, we demonstrated that (1) could significantly inhibit proliferation of hepatoma cell lines, which is related to mainly arrest the cell cycle at G0/G1 phase. Complex (1) and mixture ((2) and (3), 1:1 molar ratio) exerted similar 50% inhibited rate from hepatoma cell lines showed that (1) might be a cooperative inhibitor with (2) and (3) toward tumor growth in solution through its hydrolyzation. Interestingly, effects of transition metal ion coordination, and numbers and types of ligand can exert key influence on the evaluation of cytotoxicity. Furthermore, we conducted the study of acute toxicity on the oral administration of (1) in ICR mice and calculated LD₅₀ value of (1) is 736 mg/kg, with the 95% confidence limits of 635-842 mg/kg. The results showed that overdosing on complex (1) might possess lower toxicity in mice. Therefore, complex (1) provided direct evidences to exploit the design of novel chemotherapeutic drugs with high antitumor activity and low toxicity. In addition, administration of complex (1) can be made by the oral/gavage route, which is not only convenient but also safe. The underlying molecular mechanisms for liver cancer treatment are being explored in our following research. We will further develop this comprehensive approach towards informed transition metal based drug design in targeted cancer therapies.

Acknowledgements

This work was supported by the National Natural Science Foundation of China (Grant No. 21401162), the Natural Science Foundation of the Jiangsu Higher Education Institutions of China (Grant No. 14KJB430024), Jiangsu Provincial Postdoctoral Sustentation Fund (Grant No. 1402015B). Financial support from the Priority Academic Program Development of Jiangsu Higher Education Institutions and the Natural Science Foundation of Education Committee of Jiangsu Province (No. 12KJB150023) is gratefully acknowledged. The authors also acknowledge the Testing Center of Yangzhou University for ESI-MS measurements.

Notes and references

- (a) *Global Cancer Facts & Figures 2007*. Atlanta GA: American Cancer Society, 2007, 1-46; (b) S. E. Atawodi, *Infet Agen Cancer*. 2011, **6**, 2-9.
- (a) V. Milacic, D. Chen, L. Ronconi, K. R. Landis-Piwowar, D. Fregona, Q. P. Dou, *Cancer Res.*, 2006, **66**, 10478-10486; (b) K. Kehe, Szinicz, L. *Toxicology*. 2005, **214**, 198-209; (c) J. J. Soldevila-Barreda, I. Romero-Canelón, A. Habtemariam, P. J. Sadler, *Nat Commun*, 2015, **6**, 6582-6591.
- (a) D. J. Higby, H. J. Wallac Jr, D. J, Albert, J. F. Holland, *Cancer*. 1974, **33**, 1219-1225. (b) B. Rosenberg, L. Van Kamp, J. F. Trosko, V. H. Mansour, *Nature*, 1969, **222**, 385-386. (c) D. B. Brown, A. R. Khokhar, M. P. Hacker, L. Lokys, J. H. Burchenal, R. A. Newman, J. J. McCormack, D. Frost, *J. Med. Chem.* 1982, **25**, 952-956. (d) U. Frey, J. D. Ranford, Sadler, P. J. *Inorg Chem*. 1993, **32**, 1333-1340. (e) T. Boulikas and M. Vougiouka, *Oncol. Rep.*, 2003, **10**, 1663-1682.
- (a) M. D. Hall, H. R. Mellor, R. Callaghan and T. W. Hambley, *J. Med. Chem.* 2007, **50**, 3403-3411; (b) E. G. Chapman, V. J. DeRose, *J. Am. Chem. Soc.*, 2010, **132**, 1946-1952; (c) S. Chen, D. Xu, H. Jiang, Z. Xi, P. Zhu, Y. Liu, *Angew. Chem. Int. Ed.* 2012, **51**, 1225-1226; (d) Đ. U. Miodragovic, J. A. Quentzel, J. W. Kurutz, C. L. Stern, R. W. Ahn, I. Kandela, A. Mazar and T. V. O'Halloran, *Angew. Chem. Int. Ed.* 2013, **52**, 10749-10752.
- (a) R. S. Go, A. A. Adjei, *J. Clin. Oncol.* 1999, **17**, 409-422; (b) D. Wang, S. J. Lippard, *Nat Rev Drug Discov* 2005, **4**, 307-320; (c) M. Dobbstein and U. Moll, *Nat Rev Drug Discov*. 2014, **13**, 1791-1796.
- (a) M. Galanski, V. B. Arion, M. A. Jakupec, and B. K. Keppler, *Current Pharmaceutical Design*, 2003, **9**, 2078-2089; (b) A. M. Kim, S. Vogt, T. V. O'Halloran, T. K. Woodruff, *Nat. Chem. Biol.*, 2010, **6**, 674-681; (c) N. Busto and B. Garcia, *Coord. Chem. Rev.*, 2013, **257**, 2848-2862; (d) M. X. Li, M. Yang, J. Y. Niu, L. Z. Zhang, S. Q. Xie, *Inorg. Chem.* 2012, **51**, 12521-12526; (e) M. Hajrezaie, K. Shams, S. Z. Moghadamtousi, H. Karimian, P. Hassandarvish, M. Emtjazjoo, M. Zahedifard, N. A. Majid, H. M. Ali, M. A. Abdulla, *Sci. Rep.* 2015, **5**, 12379.
- (a) D. L. Ma, H. -Z. He, K. -H. Leung, D. S. -H. Chan, C. -H. Leung, *Angew. Chem. Int. Ed.* 2013, **52**, 7666-7682; (b) S. Phongtongpasuk, S. Paulus, J. Schnabl, R. K. Sigel, B. Spingler, M. J. Hannon, E. Freisinger, *Angew. Chem. Int. Ed.* 2013, **52**, 11513-11516; (c) A. N. Kate, A. A. Kumbhar, A. A. Khan, P. V. Joshi, and V. G. Puranik, *Bioconjugate Chem.* 2014, **25**, 102-114; (d) A. de Almeida, B. L. Oliveira, J. D.G. Correia, G. Soveral, A. Casini, *Coord. Chem. Rev.*, 2013, **257**, 2689-2704; (e) C. Santini, M. Pellei, V. Gandin, M. Porchia, F. Tisato and C. Marzano, *Chem. Rev.* 2014, **114**, 815-862; (f) E. -J. Kim, S. Bhuniya, H. Lee, H. M. Kim, C. Cheong, S. Maiti, K. S. Hong and J. S. Kim, *J. Am. Chem. Soc.* 2014, **136**, 13888-13894.
- J. A. Drewry, P. T. Gunning, *Coord. Chem. Rev.*, 2011, **255**, 459-472.
- Y. Yoshikawa and H. Yasui, *Curr. Top. Med. Chem.*, 2012, **12**, 210-218
- (a) Q. Jiang, J. Zhu, Y. Zhang, N. Xiao and Z. Guo, *BioMetals*, 2008, **22**, 297-305; (b) S. Anbu, S. Kamalraj, B. Varghese, J. Muthumary, and M. Kandaswamy, *Inorg Chem*, 2012, **51**, 5580-5592.
- (a) M. Terenzi, G. Fanelli, G. Ambrosi, S. Amatori, V. Fusi, L. Giorgi, V. Turco Liveri and G. Barone, *Dalton Trans.*, 2012, **41**, 4389-4395; (b) Y. Nakamura, Y. Taruno, M. Sugimoto, Y. Kitamura, H. L. Seng, S. M. Kong, C. H. Ng and M. Chikira, *Dalton Trans.*, 2013, **42**, 3337-3345.
- (a) C. -H. Ng, K. C. Kong, S. T. Von, P. Balraj, P. Jensen, E. Thirthagiri, H. Hamada and M. Chikira, *Dalton Trans.*, 2008, 447-454; (b) L. -F. Chin, S. -M. Kong, H. -L. Seng, Y. -L. Tiong, K. -E. Neo, M. J. Maah, A. S. -B. Khoo, M. Ahmad, T. -S. A. Hor, H. -B. Lee, S. -L. San, S. -M. Chye and C. -H. Ng, *J. Biol. Inorg.*

- Chem.* 2012, **17**, 1093-1105; (c) H. -L. Ng, C. -H. Ng, and S. -W. Ng, *Acta Cryst.* 2009, **E65**, m89. (d) H. L. Seng, H. K. A. Ong, R. N. Z. R. A. Rahman, B. M. Yamin, E. R. T. Tiekink, K. W. Tan, M. J. Maah, I. Caracelli, and C. -H. Ng, *J Inorg Biochem*, 2008, **102**, 1997-2011; (e) L. -F. Chin, C. -H. Ng, and S. -W. Ng, *Acta Cryst.* 2009, **E65**, m40; (f) W. -Y. Huang, Z. -L. Chen, H. -H. Zou, D.-C. Liu, F. -P. Liang, *Polyhedron*. 2013, **50**, 1-9.
- 13 (a) S. Jagadeesan, V. Balasubramanian, P. Baumann, M. Neuburger, D. Häussinger, and C. G. Palivan, *Inorg. Chem.*, 2013, **52**, 12535-12544; (b) D. Wesselinova, M. Neykov, N. Kaloyanov, R. Toshkova and G. Dimitrov, *Eur. J. Med. Chem*, 2009, **44**, 2720-2723; (c) S. Ambika, S. Arunachalam, R. Arun and K. Premkumar, *RSC Adv.*, 2013, **3**, 16456-16468; (d) S. Anbu, M. Kandaswamy, S. Kamalraj, J. Muthumarry and B. Varghese, *Dalton Trans.*, 2011, **40**, 7310-7318; (e) S. Roy, K. D. Hagen, P. U. Maheswari, M. Lutz, A. L. Spek, J. Reedijk, G. P. van Wezel, *ChemMedChem*. 2008, **3**, 1427-1434.
- 14 (a) B. Selvakumar, V. Rajendiran, P. U. Maheswari, H. Stoeckli-Evans, M. Palaniandavar, *J Inorg Biochem*, 2006, **100**, 316-330; (b) C. Yuan, M. Zhu, Q. Wang, L. Lu, S. Xing, X. Fu, Z. Jiang, S. Zhang, Z. Li, Z. Li, R. Zhu, L. Ma. *Chem. Commun.*, 2012, **48**, 1153-1155.
- 15 L. B. Ni, R. H. Zhang, Q. X. Liu, W. S. Xia, H. X. Wang, Z. H. Zhou, *J. Solid State Chem.*, 2009, **182**, 2698-2706.
- 16 N. -H. Hu, Y. -S. Liu, *Acta Cryst.* 1991, **47**, 2324-2326.
- 17 Oxford Diffraction, CrysAlis CCD and CrysAlis RED, Oxford Diffraction Ltd., Abingdon, UK, 2005.
- 18 L. J. Farrugia, *J. Appl. Crystallogr.* 1999, **32**, 837-838.
- 19 G. M. Sheldrick, SHELX97, *Programs for Crystal Structure Analysis*; Release 97-2; University of Göttingen, Göttingen: Germany, 1997.
- 20 H. Yang, C. Liu, Y. Q. Zhang, L. T. Ge, J. Chen, X. Q. Jia, R. X. Gu, Y. Sun, W. D. Sun, *Int Immunopharmacol.* 2015, **24**, 423-431.
- 21 (a) H. B. Xu, Y. H. Zhao, Z. M. Su, G. H. Li, Y. Ma, K. Z. Shao, D. X. Zhu, H. J. Zhang, S. M. Yue, *Chem. Lett.* 2004, **33**, 446-447; (b) A. C. Morel, D. Choquesillo-Lazarte, C. Alarcón-Payer, J. M. González-Pérez, A. Castiñeiras, J. Nicolás-Gutiérrez. *Inorg. Chem. Commun.* 2003, **6**, 1354-1357; (c) S. W. Jin, D. Q. Wang, W. Z. Chen, *Inorg. Chem. Commun.* 2007, **10**, 685-689.
- 22 (a) L. J. Barbour, G. W. Orr, J. L. Atwood, *Nature*, 1998, **393**, 671-673; (b) M. Oshizawa, K. S. Kurihara, N. Niimura, M. Fujita. *J. Am. Chem. Soc.*, 2005, **127**, 2798-2799; (c) L.-Y. Wang, Y. Yang, K. Liu, B. -L. Li, and Y. Zhang, *Cryst. Growth Des.*, 2008, **8**, 3902-3904; (d) L. J. Barbour, G. W. Orr and J. L. Atwood, *Chem. Commun.*, 2000, 859-860.
- 23 (a) M. -L. Wei, C. He, W. -J. Hua, C. -Y. Duan, S. -H. Li, Q. -J. Meng, *J. Am. Chem. Soc.* 2006, **128**, 13318-13319; (b) P. S. Lakshminarayanan, E. Suresh, and P. Ghosh, *J. Am. Chem. Soc.* 2005, **127**, 13132-13133; (c) D. Sun, D. -F. Wang, N. Zhang, R. -B. Huang, and L. -S. Zheng, *Cryst. Growth Des.*, 2010, **10**, 5031-5033.
- 24 (a) S. Metzger, B. Lippert, *J. Am. Chem. Soc.* 1996, **118**, 12467-12468; (b) R. A. Musah, G. M. Jensen, R. J. Rosenfeld, D. E. McRee, D. B. Goodin, S. W. Bunte, *J. Am. Chem. Soc.* 1997, **119**, 9083-9084; (c) T. Steiner, W. Saenger, *J. Am. Chem. Soc.* 1993, **115**, 4540-4547.
- 25 (a) J. Morizzi, M. Hobday and C. Rix, *J. Mater. Chem.*, 2001, **11**, 794-798; (b) R. Clarke, K. Latham, C. Rix, M. Hobday and J. White, *CrystEngComm*, 2004, **6**, 42-50; (c) O. O. Litsis, V. A. Ovchinnikov, V. P. Scherbatskii, S. G. Nedilko, T. Y. Sliva, V. V. Dyakonov, O. V. Shishkin, V. I. Davydov, P. Gawryszewska and V. M. Amirkhanov, *Dalton Trans.*, 2015, **44**, 15508-15522.
- 26 (a) A. Patra, T. K. Sen, R. Bhattacharyya, S. K. Mandal and M. Bera, *RSC Adv.*, 2012, **2**, 1774-1777; (b) S. K. Papageorgiou, E. P. Kouvelos, E. P. Favvas, A. A. Sapalidis, G. E. Romanos, F. K. Katsaros, *Carbohydr Res*, 2010, **345**, 469-473.
- 27 (a) A. D'Aléo, E. Cecchetto, L. D. Cola, R. M. Williams, *Sensors* 2009, **9**, 3604-3626; (b) S. -G. Roh, Y. -H. Kim, K. D. Seo, D. H. Lee, H. K. Kim, Y. Park, J. -W. Park, and J. -H. Lee, *Adv. Funct. Mater.* 2009, **19**, 1663-1671; (c) Z. Mao, W. Senevirathna, J. -Yu Liao, J. Gu, S. V. Kesava, C. Guo, E. D. Gomez, and G. Sauvé, *Adv. Mater.* 2014, **26**, 6290-6294; (d) H. Xu, R. Chen, Q. Sun, W. Lai, Q. Su, W. Huang and X. Liu, *Chem. Soc. Rev.*, 2014, **43**, 3259-3302; (e) W. Senevirathna, J. -Yu. Liao, Z. Mao, J. Gu, M. Porter, C. Wang, R. Fernando and G. Sauvé, *J. Mater. Chem. A*, 2015, **3**, 4203-4214.
- 28 Z. Xu, J. Yoon, D. Spring, *Chem. Soc. Rev.*, 2010, **39**, 1996-2006.
- 29 (a) X. Shi, G. Zhu, X. Wang, G. Li, Q. Gand, X. Zhao, G. Wu, G. Tian, M. Xue, R. Wang, S. Qiu, *Cryst. Growth Des.* 2004, **5**, 341-346; (b) T. L. Hu, R. Q. Zou, J. R. Li, X. H. Bu, *Dalton Trans.*, 2008, 1302-1311; (c) Z. Liu, W. He, Z. Guo, *Chem. Soc. Rev.*, 2013, **42**, 1568-1600.
- 30 (a) K. Binnemans, *Chem. Rev.* 2009, **109**, 4283-4374; (b) R. G. Xiong, J. L. Zuo, X. Z. You, B. F. Abrahams, Z. P. Bai, C. M. Che, H. K. Fun. *Chem. Commun.*, 2000, 2061-2062; (c) J. Z. Wang. *Anorg. Allg. Chem.* 2011, **637**, 1612-1615.
- 31 (a) G. A. Naganagowda, K. V. Ramanathan, V. Gayathri and N. M. Nanjegowda, *Magn. Reson. Chem.* 2000, **38**, 223-228; (b) D. Sorsche, C. Pehlken, C. Baur, S. Rommel, K. Kastner, C. Streb and S. Rau, *Dalton Trans.*, 2015, **44**, 15404-15407.
- 32 (a) L. F. Qin, I. O. Ng, *Cancer Lett.* 2002, **175**, 27-38; (b) Z. Feng, Y. Lai, H. Ye, J. Huang, X. G. Xi, Z. Wu, *Cancer Sci.* 2010, **101**, 2476-2482; (c) G. -Q. Li, X. -G. Chen, X. -P. Wu, J. -D. Xie, Y. -J. Liang, X. -Q. Zhao, W. -Q. Chen, and L. -W. Fu, *PLoS One.* 2012, **7**, e48994; (d) H. Du, W. Yang, L. Chen, M. Shi, V. Seewoo, J. Wang, A. Lin, Z. Liu, W. Qiu, *Oncol Rep.* 2012, **27**, 143-150.
- 33 (a) J. F. Kou, C. Qian, J. Q. Wang, X. Chen, L. L. Wang, H. Chao, L. N. Ji. *J Biol Inorg Chem.* 2012, **17**, 81-96; (b) F. Wang, L. He, W. Q. Dai, Y. P. Xu, D. Wu, C. L. Lin, S. M. Wu, P. Cheng, Y. Zhang, M. Shen, C. F. Wang, J. Lu, Y. Q. Zhou, X. F. Xu, L. Xu, C. Y. Guo. *PLoS One.* 2012, **7**, e50638.
- 34 P. Heffeter, M. A. Jakupc, W. Körner, S. Wild, N. G. V. Keyserlingk, L. Elbling, H. Zorbas, A. Korynevskaya, S. Knasmüller, H. Sutterlüty, *Biochem Pharmacol.* 2006, **71**, 426-440.
- 35 Q. Xin, Z. Y. Ma, C. Z. Xie, X. Fei, Y. W. Zhang, J. Y. Xu, Z. Y. Qiang, J. S. Lou, G. J. Chen, S. P. Yan, *J. Inorg. Biochem.* 2011, **105**, 728-737.
- 36 P. Venkatesan, N. Puvvada, R. Dash, K. Prashanth, D. Sarkar, B. Azab, *Biomaterials*, 2011, **32**, 3794-3806.
- 37 C. Liu, W. Zhang, H. Yang, W. D. Sun, X. D. Gong, J. X. Zhao, Y. Sun, and G. W. Diao, *PLOS One.* 2014. **9**, e10176.
- 38 (a) M. P. Hacker, A. R. Khokhar, I. H. Krakoff, D. B. Brown, J. J. McCormack, *Cancer Res.* 1986, **46**, 6250-6254; (b) Y. Yu, L. G. Lou, W. P. Liu, H. J. Zhu, Q. S. Ye, X. Z. Chen, W. G. Gao, S. Q. Hou, *Eur J Med Chem.* 2008, **43**, 1438-1443.
- 39 X. H. Huang, P. C. Xiong, C. M. Xiong, Y. L. Cai, A. H. Wei, J. P. Wang, X. F. Liang, J. L. Ruan, *Phytomedicine.* 2010. **17**, 930-934.
- 40 P. S. Randhawa, R. Shapiro, M. L. Jordan, T. E. Starzl, A. J. Demetris, *Am J Surg Pathol.* 1993, **17**, 60-68.